MASTERARBEIT | MASTER'S THESIS

Titel | Title

Establishment of Primary Microglia Isolation, Culture and Phagocytosis Protocol for Adult Mouse Brain

verfasst von | submitted by

Lea Egerer BSc MSc

angestrebter akademischer Grad | in partial fulfilment of the requirements for the degree of

Master of Science (MSc)

Wien | Vienna, 2024

Studienkennzahl lt. Studienblatt | Degree programme code as it appears on the student record sheet:	UA 066 834
Studienrichtung lt. Studienblatt | Degree programme as it appears on the student record sheet:	Masterstudium Molekulare Biologie
Betreut von | Supervisor:	Univ.-Prof. Mag. Dr. Johannes Berger

1. Acknowledgements

Firstly, I would like to thank my supervisor Prof. Johannes Berger for guiding me through this process with patience, knowledge, and advice. Secondly, I would like to thank my colleagues Charlotte Brexc, Arthur Vansimpsen, Bianca Hafner, Andrea Villoria-Gonzales and Anna Wunder, who made my time in the lab not only more efficient but significantly more fun. Thirdly, I would like to extend thanks to Martina Rothe, who always made time to help and support me and without whom this Thesis would not have been possible. Furthermore, I would like to thank Isabelle Weinhofer for supporting me with great advice and knowledge even though she was not my supervisor. Lastly, I want to give thanks to my family, who have supported me both financially and emotionally throughout my life and specifically my studies. They have encouraged me to always be myself and to pursue my interests and passions, whatever those might have been. Special thanks go out to Raphael Schreiner, who motivated me to work harder and realize my full potential. I could not have done it without you.

2. Abstract

Ether lipids, particularly plasmalogens, are significant in various cellular processes, highlighting their crucial role in membrane stability and function. Clinical manifestations of disorders associated with ether lipid deficiencies emphasize their impact on brain development and function. This study presents a tool to investigate the role of primary microglia phagocytosis of myelin debris, aiming to unravel their implications in neuroinflammatory processes.

Primary microglia were isolated using enzymatic dissociation, magnetic bead labelling and their purity was assessed via flow cytometry and immunofluorescent staining. Highly pure myelin was isolated from adult mouse brain and labelled with pHrhodo green dye to use as a substrate for the following phagocytosis assay. Phagocytosis of fluorescently labelled myelin by isolated primary microglia was measured with the IncuCyte live-imaging system.

Flow cytometry analysis revealed an average microglia purity of 93% and CD11b-stainings confirmed the cell identity of the isolated microglia. After four days in cell culture, the isolated microglia showed cell type specific processes. WT microglia performed phagocytosis of labelled myelin particles with a peak at 12 to 15 hours after substrate addition and a linear decline in phagocytosis within 48 hours.

This study establishes a robust microglia isolation protocol from adult murine brains, facilitating neuroimmunology research. Methodological optimizations enhance purity and reproducibility, laying groundwork for investigating microglia in various contexts, from neuroinflammation to neurodegeneration. The findings underscore the importance of methodological rigor in microglia isolation, providing a foundation for advancing our understanding of microglia biology in health and disease.

3. Zusammenfassung

Etherlipide, insbesondere Plasmalogene, spielen eine wichtige Rolle bei verschiedenen zellulären Prozessen und betonen ihre entscheidende Bedeutung für die Membranstabilität und -funktion. Klinische Manifestationen von Störungen im Zusammenhang mit Etherlipidmangel unterstreichen ihre Auswirkungen auf die Gehirnentwicklung und -funktion. In dieser Studie wurde eine Methode zur Untersuchung der Rolle der primären Mikroglia-Phagozytose von Myelinresten entwickelt und zielt darauf ab, deren Auswirkungen auf neuroinflammatorische Prozesse aufzuklären.

Primäre Mikroglia wurden mittels enzymatischer Dissoziation und magnetischer Antikörper isoliert, und ihre Reinheit wurde mittels Durchflusszytometrie analysiert. Aufgereinigtes Myelin wurde aus dem Gehirn erwachsener Mäuse isoliert und mit pHrhodo-Grün markiert, welches erst fluoresziert, sobald es in das Lysosom der Zellen aufgenommen wurde. Die Phagozytose von fluoreszenzmarkiertem Myelin durch isolierte primäre Mikroglia wurde mit dem IncuCyte-Live-Imaging-System gemessen.

Die Durchflusszytometrie-Analyse ergab eine durchschnittliche Mikroglia-Reinheit von 93%, und CD11b-Färbungen bestätigten die Zellidentität der isolierten Mikroglia. Nach vier Tagen in Zellkultur zeigten die isolierten Mikroglia zellspezifische Prozesse. WT-Mikroglia führten die Phagozytose von markierten Myelinpartikeln mit einem Höhepunkt nach 12 bis 15 Stunden nach Zugabe des Substrats und einem linearen Rückgang der Phagozytose innerhalb von 48 Stunden durch.

Diese Studie etabliert ein robustes Mikroglia-Isolationsprotokoll aus erwachsenen murinen Gehirnen, das die neuroimmunologische Forschung erleichtert. Methodische Optimierungen verbessern Reinheit und Reproduzierbarkeit und legen damit den Grundstein für die Erforschung von Mikroglia in verschiedenen Kontexten, von der Neuroinflammation bis zur Neurodegeneration. Die Ergebnisse unterstreichen die Bedeutung methodischer Standardisierung bei der Isolierung von Mikroglia und bieten eine Grundlage für das Voranschreiten unseres Verständnisses von Mikroglia-Biologie in Gesundheit und Krankheit.

4. Contents

5. Introduction

5.1. Ether lipids

Essential for ether lipid synthesis are subcellular organelles called peroxisomes. These are present in all major eukaryotic species, however, next to core metabolic functions they serve different additional purposes between species (Smith & Aitchison, 2013). The peroxisome´s function in mammals and especially humans ranges from oxidation of fatty acids to the synthesis of ether lipids, which is a complex process involving a multitude of enzymes and pathways (Wanders & Waterham, 2006). As can be seen in Figure 1, the rate-limiting enzyme that is involved in the synthesis of ether lipids is the FAR1 enzyme, which is responsible for the production of fatty alcohols (Honsho et al., 2013). Within the peroxisome, two sequentially acting enzymes dihydroxyacetone phosphate acyltransferase (DHAPAT; EC 2.3.1.42; gene name: glycerone phosphate acyltransferase, GNPAT) and alkyl-dihydroxyacetone phosphate synthase (ADHAPS) are responsible for generating the ether bond. Through an unknown mechanism of exit, modifications of ether lipid precursors are completed within the ER or the cytosol (Dorninger et al., 2020). Two types of peroxisomal disorders can be described in humans, namely single peroxisomal enzyme deficiencies and peroxisome biosynthesis disorders (PBD) (Waterham & Ebberink, 2012).

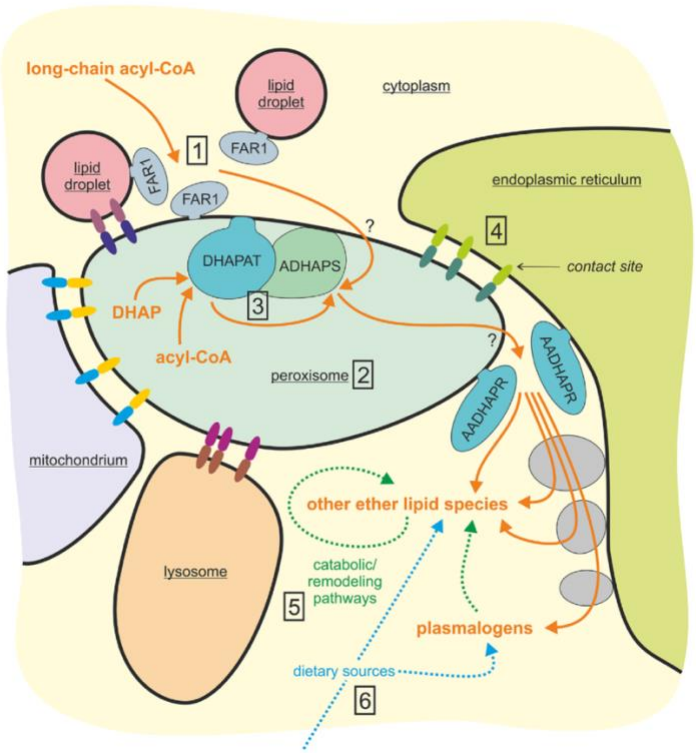

Figure 1: Biosynthesis of ether lipids in the peroxisome and surrounding organelles. Figure acquired from Dorninger et al. (2020).

The most common type of single peroxisomal enzyme deficiencies is X-Adrenoleukodystrophy (X-ALD), which is characterized by a defect in transferring the fatty acids into the peroxisome, resulting in a pathological accumulation of VLCFAs in the cytosol. Patients with X-ALD exhibit a heterogenous phenotype including adrenal insufficiency, progressive demyelination and paraparesis (Björn M van Geel et al., 1997). PBD on the other hand are brought about by dysfunction of the PEX gene family, which are responsible for peroxisome biogenesis. The most common type of human PBD are the Zellweger spectrum disorders (ZSD), which represent a spectrum of disorders with varying degrees of diminished peroxisomes in patients. Zellweger syndrome, as the most severe form of ZSD, is characterized by dysfunction of neuronal migration and overall brain development and function (Björn M van Geel et al., 1997).

Congenital ether lipid synthesis defects in humans lead to the rare disease rhizomelic chondrodysplasia punctata (RCDP), which can be divided into five different subtypes with varying genetic differences and has a prevalence of 1:100000. In general, hallmarks of RCDP are shortening of proximal long bones, developmental retardation, cataracts, and structural abnormalities in the brain including myelination deficits (Duker et al., 2020). The disorder exhibits clinical

heterogeneity, displaying a diverse spectrum of severity and manifestations. Clinical symptoms encompass symmetrical shortening of proximal limbs, joint contractures, and a distinctive dysmorphic facial appearance. Additional indications comprise cataracts, impaired hearing, and psychomotor retardation. Radiographically, anomalies are observed, such as calcified stippling of epiphyses, shortened femora and humeri with epi-metaphyseal widening, and coronal clefts in most vertebral bodies (Alkan et al., 2003). Severity of symptoms varies between lethal forms occurring already in the neonatal period and less severe forms that may allow patients to survive until adolescence, depending on the individual access to health care. Currently there is no cure for RCDP with the main approach to treatment being to alleviate symptoms and improve the patient's quality of life. Due to the variability of disease symptoms diagnosis of the disease is often challenging for practitioners (Braverman & Moser, 2012a).

Presently, there are five recognized subtypes of RCDP, each attributed to a specific genetic mutation. RCDP type 1, the most prevalent subtype accounting for 90% of RCDP cases, results from a mutation in the PEX7 gene. This gene is responsible for the cytosolic receptor for proteins containing PTS2. Consequently, proteins with a PTS2 signal sequence, including AGPS, are unable to enter the peroxisome, leading to a deficiency of essential proteins. RCDP types 2 and 3 both involve mutations in genes responsible for the ether bond in ether lipid biosynthesis. Specifically, RCDP type 2 stems from a GNPAT mutation, while type 3 arises from a mutation in the AGPS gene. RCDP type 4 is associated with a mutation in FAR1, encoding for FAR1 enzyme. Notably, this subtype of RCDP exhibits a milder phenotype due to compensation by FAR2. Lastly, RCDP type 5 results from a PEX5L mutation, and PEX5L belongs to the PEX5 family. PEX5 encodes for a cytosolic protein that functions as a receptor for peroxisomal matrix proteins containing a PTS1. The PEX5L splice variant also acts as a co-receptor for PTS2-containing matrix proteins (Barøy et al., 2015; Duker et al., 2017). In all these subtypes, studies showed, that the reduction of ethanolamine plasmalogens goes hand in hand with an increase in phosphatidylethanolamine. Other phospholipids however, did not show any differences in concentrations, indicating that plasmalogen insufficiency is partially compensated in RCDP by phosphatidylethanolamine (Dorninger et al., 2015).

5.1.1. Plasmalogens

The distinction between non-plasmalogen ether lipids and plasmalogens is based on the characteristic vinyl-ether bond at the sn1-position, as can be seen in Figure 2. The ether bond of all ether lipids is facilitated by the activity of the GNPAT enzyme, which introduces it within the peroxisome. After exiting the peroxisome, the vinyl ether bond is formed by the PEDS1 enzyme in the ER (Werner et al., 2020). Plasmalogens can be further categorized into different subtypes by the nature of their headgroup. The most abundant of these are plasmalogen ethanolamines and plasmalogen cholines.

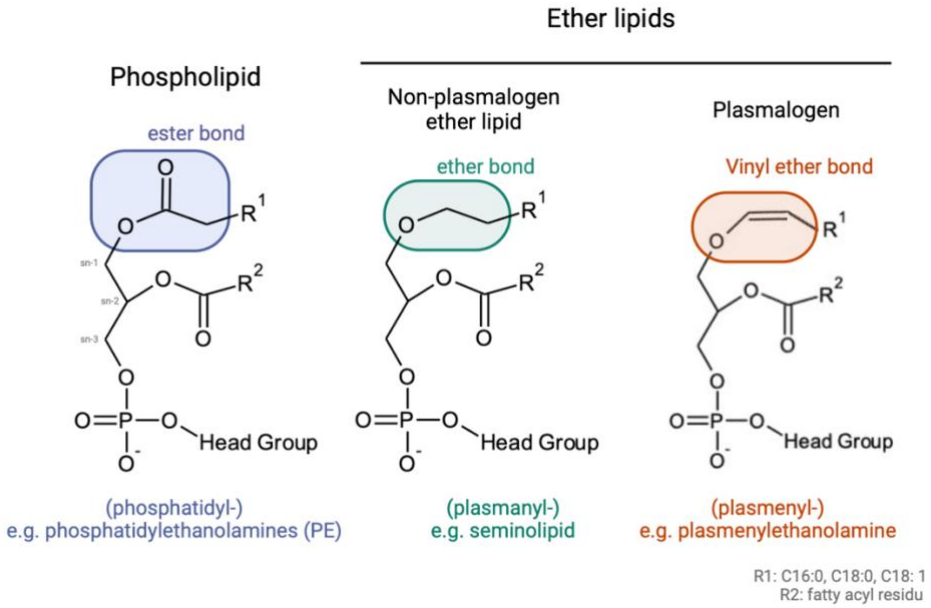

Figure 2: overview of structural differences in ether lipids. Distinction between plasmalogens and ether lipids through the vinyl ether bond at the sn1-position of the plasmalogens versus an ether bond in other ether lipids. Figure was provided by Charlotte Brexc.

Plasmalogens constitute the most abundant ether lipids in the brain, comprising approximately 20% of all lipids, and are present to a lesser extent in liver and heart tissues. Initially, plasmalogens were primarily attributed to antioxidative defense; however, recent insights highlight their crucial role as integral membrane constituents. Consequently, plasmalogens contribute to membrane stability and play a significant role in dynamic cellular processes such as endocytosis. The absence of plasmalogens imposes considerable stress on cells, altering membrane properties. Studies indicate that modifications to the vinyl ether bond have profound effects on the formation of the lipid bilayer, which is universally present in cells. Additionally, *in vitro* experiments demonstrate that increasing the concentration of

plasmalogens promotes the fusion rate of lipid vesicles, underscoring their essential role in the proper functioning of curved lipid membranes (Koivuniemi, 2017).

Supporting these findings, plasmalogens significantly influence neurotransmitter release in the central nervous system (CNS). Given that neurotransmission is contingent upon the proper functioning of the synaptic vesicle cycle, which facilitates neuronal communication, lipids play a pivotal role (Davletov & Montecucco, 2010). Notably, plasmalogens are prominent constituents of the synapse membrane (Hofteig et al., 1985) and synaptic vesicles (Takamori et al., 2006). The role of plasmalogens in signaling has garnered increased interest due to their enrichment in "lipid rafts," microdomains known to compartmentalize signal transduction and particularly rich in plasmalogens. These lipid rafts are hypothesized to organize and sequester SNARE proteins, thereby contributing to the mediation of exocytosis during neurotransmitter release (Pike, 2006).

Moreover, plasmalogens have been implicated in dysfunction within the AKT signaling cascade, leading to demyelination. The absence of plasmalogens is associated with defective protein kinase B (AKT) phosphorylation, resulting in increased activation of glycogen synthase kinase 3b (GSK3b) in nerves of mutant mice. Schwann cell defects include untimely differentiation and impaired myelination. This provides further evidence that plasmalogens play a pivotal role in regulating membrane function and cell signaling (Da Silva et al., 2014).

5.1.2. Pathologies

With Alzheimer´s Disease (AD) as the most prevalent form of dementia and its rising problem in health care and society, finding markers and non-invasive strategies of detection has come to the forefront of AD research. Specific choline phospholipid species have been suggested as a possible target since altered levels of phospholipids circulating in the plasma of patients have been found in connection to AD development (Mapstone et al., 2014). Regarding the specific role of plasmalogens in AD, in the white matter of post-mortem brains of sAD patients, reduced levels of PlsEtn have been discovered (Han et al., 2001). Apart from that, a lack of PlsEtn in the plasma of spontaneous AD patients could be linked to their progressive cognitive decline (Han, 2005). A study by Dorninger et al. (2018) quantified specific choline phospholipids, identified as potential Alzheimer's disease (AD) biomarkers. Their findings indicate, that during normal aging,

lysophosphatidylcholine, choline plasmalogen, and lyso-platelet activating factor levels significantly increase. Importantly, individuals developing probable AD exhibit more pronounced changes, suggesting that the conversion to AD resembles an accelerated aging process for choline-containing plasma phospholipids.

Next to neurodegenerative diseases like AD, RCDP in mild form has been linked to psychiactric disorders like autistic behavior and hyperactivity, with a confirmed genetic link (Dorninger et al., 2019). This association is supported by the analysis of plasma from autistic patients, revealing diminished plasmalogen levels (Wiest et al., 2009). Consequently, there is a presumption that ether lipids and plasmalogens may contribute to the etiology of some psychiatric disorders. Mouse model experiments, particularly the RCDP mouse model, have validated these observations, demonstrating significant behavioral differences akin to those observed in mice displaying autistic behavior (Dorninger, Zeitler, et al., 2020).

5.2. Mouse models of ether lipid deficiencies

As the first to describe a ether lipid deficient mouse model, Rodemer et al., (2003) characterized the phenotypic hallmarks of *Gnpat* KO mice, revealing critical insights into the functional consequences of disrupting the glyceronephosphate O-acyltransferase (*Gnpat*) gene. Their *in vitro* model demonstrated a profound absence of ether lipids in the *Gnpat* KO mice, emphasizing the pivotal role of the Gnpat enzyme in ether lipid biosynthesis. Interestingly, male infertility emerged as a notable consequence of Gnpat deficiency in mice, shedding light on the broader physiological implications of ether lipid dysregulation, mainly due to the absence of seminolipids, which are an integral part of male fertility. Additionally, the *Gnpat* KO mice exhibited defects in eye development, presenting with cataract formation and optic nerve hypoplasia. *Gnpat* KO mice are further characterized by their low body weight and small stature, which is also commonly observed in RCDP patients.

Regarding the behavioral phenotype of Gnpat KO mice, altered social behaviors have been observed. In the marble burying test, which is commonly used to test for neurodevelopmental disorders, *Gnpat* KO mice behave differently to WT mice. Where WT mice quickly bury the marbles, that are placed in their cages, *Gnpat* KO mice fail to do so, therefore displaying a phenotype that is observed in ASD and attention deficit hyperactivity disorder (ADHD) mouse models (Dorninger, Gundacker, et al., 2019). In connection to these findings, *Gnpat* KO mice showed a

dysfunction in their neuromuscular junction (NMJ) (Han, 2005) as well as in neurotransmitter homeostasis, which serve as an explanation for the progressive tremors and generalized ataxia in these mice (Dorninger, König, et al., 2019). These findings underscore the critical role of GNPAT in orchestrating various cellular processes, providing a valuable model for further investigations into the molecular mechanisms underlying RCDP type 2 and associated phenotypes.

Recently, the targeted knockout (KO) of the *Peds1* gene in mice was achieved, providing valuable insights into the role of this gene in cellular processes. The *Peds1* gene, crucial for the formation of the vinyl-ether bond exclusive to plasmalogens, emerges as a pivotal player in lipid metabolism (Werner et al., 2020). Notably, *Peds1* KO mice exhibited a significant reduction in body weight, highlighting the potential impact of *Peds1* deficiency on overall metabolic regulation. Surprisingly, despite the weight difference, *Peds1* KO mice demonstrated fertility, deviating from the reproductive challenges observed in other genetic models. In contrast to the phenotype observed in *Gnpat* KO mice, the absence of cataracts in *Peds1* KO mice suggests a unique relationship between *Peds1* and ocular development. However, subtle abnormalities manifested in various systems, including eye morphology and pigmentation, as well as skeletal and hematopoietic systems. Intriguingly, no discernible behavioral abnormalities have been identified thus far in *Peds1* KO mice (Ingham et al., 2019). Given the recent discovery of these mice, ongoing research endeavors aim to comprehensively explore the behavioral aspects, providing a comprehensive understanding of the physiological consequences associated with *Peds1* deficiency. This lays the foundation for a nuanced comprehension of the intricate interplay between *Peds1*, lipid metabolism, and broader physiological homeostasis.

5.3. Microglia

5.3.1. Functions in the CNS

Already in 1932, Del Rio-Hortega discovered the basics of microglia function. He found that initially, microglia infiltrate the developing brain with an amoeboid morphology, originating from mesodermal cells in the yolk sac. Their migration is guided by vessels and white matter tracts, allowing them to extensively populate all regions of the brain. As the brain matures, these microglia transition into a ramified, branched phenotype, commonly referred to as resting microglia. In the mature brain,

they exhibit a uniform distribution across the central nervous system, each cell occupying a defined territory. However, following a pathological event, a transformative process occurs, leading to a return to an amoeboid morphology reminiscent of their early developmental stage. Intriguingly, these transformed microglia retain the capacity for migration, proliferation, and phagocytosis, underscoring their versatile role in responding to and resolving neurobiological challenges.

5.3.2. Phagocytosis

Phagocytosis in general describes the process of specific types of cells finding and digesting debris and cells of all kinds. The cells or debris that needs to be removed will send out “find me”, “eat me” and “digest me” signals, which can be detected by specialized immune cells. To properly digest cells and debris, the immune cells must extend their plasma membrane around the particle they need to get rid of and then this debris-filled vesicle must be successfully endocytosed (Flannagan et al., 2012). Phagocytosis in the CNS is mainly taken care of by professional phagocytes like the resident microglia in the brain, which constantly scan the environment for possible debris. CNS phagocytosis mainly focuses on eliminating unnecessary synapses, apoptotic cells and debris that stems from the normal aging processes that take place in the brain (Galloway et al., 2019). If microglia activation exceeds a threshold, a signal will be sent to bone-marrow-derived macrophages (BMDMs) in the periphery, which then will be recruited into the brain for additional help during phagocytosis. Microglia and macrophages are considered professional phagocytosis cell types in the CNS (Kopper & Gensel, 2018). Recently it was revealed, that different types of macrophages clear distinctly different types of debris depending on the tissue they originate from and the area in which they act (Roberts et al., 2017).

In the developing central nervous system (CNS), phagocytosis is crucial for synaptic connectivity refinement, addressing the overproduction of neurons and synapses (Schafer & Stevens, 2013). Microglia play a pivotal role in pruning synaptic connections through immune signaling pathways, including the complement pathway, and sensing neuronal activity via nucleotides (Stephan et al., 2012). Studies focusing on the visual system underscore the significance of neuronal activity in synaptic pruning by microglia, with ADP receptor P2Y12 and CX3CR1

playing potential roles as "find me" signals (Sipe et al., 2016). The classical complement system, TREM2, and CD47-SIRPα signaling pathways also contribute to microglial synapse pruning (Filipello et al., 2018). Notably, astrocytes, mediated by receptors MerTK and MEGF10, actively participate in synaptic refinement in the developing visual system and human CNS (Chung et al., 2013). The Alzheimer-associated gene ApoE influences astrocytic phagocytic capacity and C1q accumulation during aging, while sleep deprivation enhances synaptic pruning by astrocytes, possibly mediated by MerTK (Bellesi et al., 2017; Chung et al., 2016).

5.3.3. Plasmalogens and microglia

Due to the plasmalogens role in retaining proper cell membrane stability and function, it stands to reason that they will also influence successful phagocytosis in the brain. A recent study on BMDMs lacking PlsEtn showed, that those BMDMs are not successfully removing opsonized zymosan particles compared to ones with normal PlsEtn levels. In the same study, an improvement in phagocytotic ability was observed, when the cells were treated with a plasmalogen substitute (lysoplasmalogen), which also lead to an increased amount of lipid rafts in those cells. This suggests, that PlsEtn significantly contribute to proper phagocytosis in BMDMs (Rubio et al., 2018). With regards to the impact of plasmalogens on microglia it has been found that plasmalogens are able to reduce inflammatory signaling cascades by suppressing TL4 endocytosis (Ali et al., 2019). In microglia cells lacking plasmalogens an increased rate of necroptosis can be commonly observed. If these microglia are treated with plasmalogen substitutes, they are less affected by necroptosis, therefore rendering plasmalogens necessary in preventing progressive damage to the tissue (Ali et al., 2022).

Since previous research has highlighted the importance of plasmalogens in neurodegenerative diseases associated with demyelination (like sAD), it is of special interest, how phagocytosis of myelin debris could possibly be influenced by the absence of plasmalogens. Contributing to the structure, stability and necessary compactness of myelin, plasmalogens were found especially enriched in this already lipid-rich tissue (Aggarwal et al., 2011). Within the professional phagocytic cells like BMDMs and microglia, a dynamic plasticity between pro- and anti-inflammatory qualities of the same cells can be observed. For example, after uptake of myelin debris, BMDMs will exhibit a more pro-inflammatory phenotype which

results in a foamy appearance and persistent neurotoxicity in the environment of this cell (Wang et al., 2015). Another study found that macrophages laden with myelin debris induce an auto-immune response, leading to further activation of T-cells, which in turn promotes demyelination even more (Bogie et al., 2011). On the other hand, for microglia and BMDMs it was found that after uptake of myelin, they will exhibit a more anti-inflammatory phenotype, which is needed for resolving the inflammatory response towards a healthy state (Liu et al., 2006).

Taken together, these findings hint at a highly complex interaction between phagocytosis of myelin and the more anti- or pro-inflammatory effect of microglia and BMDMs in the CNS with regards to the role of plasmalogens in these processes.

6. Objectives

The overall goal of this project in which thesis is involved in is to examine the physiological functions of plasmalogens and non-plasmalogen ether phospholipids in brain development and activities, utilizing two distinct mouse models. The initial model, involving *Gnpat* KO mice, presents a complete absence of all ether lipids, serving as a model for RCDP type 2. In contrast, the second model employs *Peds1* KO mice, featuring a targeted inactivation of the gene responsible for the vinyl ether bond in ether lipids, specifically characterizing plasmalogens.

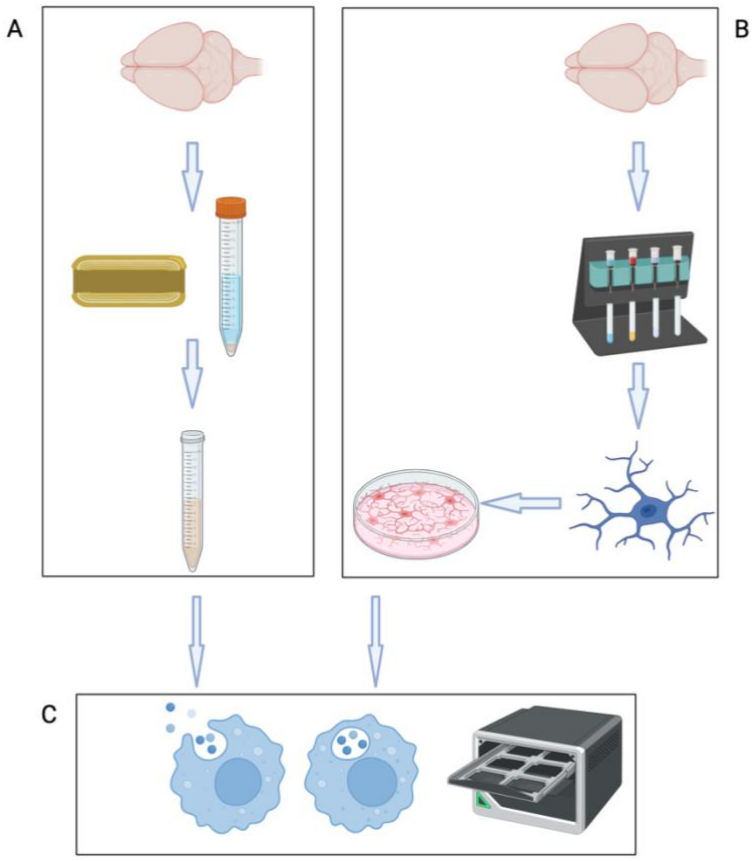

Figure 3: scheme of the workflow for the experiments. A) frozen dissected mouse brains from all genotypes were used for isolation of highly pure myelin and labelled with phRodo green as a substrate for the phagocytosis assay. B) primary microglia were isolated from freshly dissected mouse brains through magnetic bead sorting. The isolated cells were then cultured for at least 5 days before phagocytosis assay. C) microglia phagocytosis of labelled myelin was analyzed using the live-cell imaging software of the IncuCyte.

In this thesis, two main methodologies should be employed to elucidate the role of plasmalogens in the phagocytosis of myelin by primary microglia. Figure 3 illustrates the isolation of myelin from *Gnpat* KO, *Peds1* KO, and WT mice to serve as a substrate for the phagocytosis assay. The isolated myelin will be checked for contamination and was labeled with pHrhodo green, a marker visible upon myelin

uptake by microglia. Primary microglia were obtained through magnetic bead sorting following the dissociation of fresh mouse brains, and these microglia were cultured for 5 days prior to the phagocytosis assay. Live-cell imaging was utilized to quantify green fluorescence, thereby determining phagocytosis ability.

Given the critical role of ether lipids and plasmalogens in maintaining proper membrane curvature and function, it is hypothesized that the deficiency in ether lipids would impact the phagocytosis process, where precise endocytosis is essential. Moreover, as proper microglial function is pivotal in clearing myelin debris resulting from demyelination—a major contributor to pathologies in ether lipid-deficient mice—it is anticipated that microglia lacking ether lipids and plasmalogens will exhibit decreased phagocytosis abilities compared to WT microglia.

7. Material and Methods

7.1. Animals

Two mouse models related to ether lipid deficiency were used. Mice with a targeted inactivation of the *Gnpat* (Rodemer er al., 2003) and *Peds1* (Werner et al., 2020) genes via knockout (KO). The genetic variation of the strain was sustained using a mix of C57BL/6 and CD1 mice, and the groups used for experimentation were produced by breeding heterozygous animals with *Gnpat* $^{-/-}$ and *Peds1*$^{-/-}$ littermates, respectively. The genotypes were determined by PCR (see below) and reconfirmed using tail clippings directly after sacrifice. The mice were provided with standard chow diet and had unlimited access to food and water. They were kept in a room at the animal facility of the Medical University of Vienna that was temperature- and humidity-controlled, with a 12-hour light-dark cycle and low levels of ambient noise. To reduce variability in the data, sex- and age-matched WT animals were used as far as possible in all experiments.

7.2. Genotyping

The tail tip clippings, which were collected for re-genotyping were processed with the KAPA Mouse Genotyping kit (Ear Kit – Sigma KK7352). The lysis mix for each sample had a volume of 100µL and consisted of 88µL PCR grade water, 10µL 10x KAPA Express Extract Buffer and 2µL KAPA Express Extract Enzyme. To each sample 100µL of this mix was added and then it was put on a Thermocycler at 75°C (lysis) for 10 minutes and 95°C (enzyme deactivation) for 5 minutes. For the following PCR analysis, the master mix consisted of different primers for *Gnpat* and Peds samples, KAPA2G fast Genotyping mix with dye and filled up with PCR grade water. The primers for *Gnpat* samples were OLI1626 (5´-CGATACCTACTTTGTCCCAATTAGC-3´), OLI1627 (5´GCTGGTCTCAAACAGCTACGTAGCTGA-3´) and OLI1628 (5´-CGCATCGCCTTCTATCGCCTTCTTG-3´). The primers for Peds1 samples were OLI2825, OLI2826 and OLI2827. For each sample, 19 µL of the master mix were put into the PCR tubes and to each 1 µL of sample was added. A negative control was included. Within the protocol in a BioRad machine, the first minute of the protocol was performed at 94°C and 35 cycles of the same temperatures were performed with 20 seconds at 94°C, 20 seconds at 60°C, 50 seconds at 72°C. The last 7 minutes were performed at 72°C. While this program was running, the 1.5%

agarose gel was prepared for the gel electrophoresis. Approximately 20 µL of sample was filled into a 1.5% agarose gel and each well with the first well being a 100bp marker and the last well being filled with the negative control. The gels ran for 1h at 100V for the big chambers and at 80V for the small chamber. The gels were then photographed in a BioRad machine and printed. The WT band was expected at 700bp for *Gnpat* samples and at 411bp for Peds samples. The KO band for *Gnpat* was at 900bp and for Peds1 at 223bp.

7.3. Myelin isolation

Purified myelin was isolated in batches of three mouse brains at a time. I should be noted that all steps in this protocol were done on ice. After the brain was weighed, a razor blade was used to mince the brain tissue in a drop of 0.3M sucrose solution until a homogenous consistency was achieved. The pooled tissue was placed in 0.3M sucrose solution and homogenized in a Dounce homogenizer using five strokes of the loose pestle and five strokes of the tight pestle. The homogenized tissue solution was transferred to a 50mL cylinder and brought up to a final volume of 36mL with 0.3M sucrose solution. At this point 200µL of this homogenate was taken for Western blot analysis of endotoxins in the myelin.

A density gradient centrifugation was performed with 6mL of the homogenate being gently layered over 6mL of a 0.83M sucrose solution and centrifuged at 75.000xg, 4°C for 30 minutes in an ultracentrifuge (Beckmann Optima LE-80K). For the ultracentrifuge, six UC-tubes with a volume of 14mL were used. The weight of each of the six tubes was adjusted since the ultracentrifuge requires exact balancing of each of the tubes. After centrifugation, three phases could be visible, the first layer was discarded, and the interphase was collected with a glass Pasteur pipette. The crude myelin fractions were collected and transferred into a beaker.

To achieve osmotic shock, the combined myelin fractions were resuspended in 21mL of 0.2M Tris-Cl buffer and homogenized using 5 strokes of the tight pestle. The myelin membranes were transferred to a beaker and filled up to 72mL with a Tris-Cl buffer solution. 12mL of the suspensions were transferred into each of the six UC-tubes and centrifuged at 75.000xg, 4°C for 15 minutes. The supernatant was discarded, and the remaining pellet was resuspended in 0.8M Tris-Cl buffer solution using a Pasteur pipette. The same homogenization step was performed as for the step before and in a beaker the homogenates were filled up to 72mL with 0.8M Tris-

Cl buffer solution. The tubes were weighed, balanced, and centrifuged at 12.000xg, 4°C for 15 minutes. The cloudy supernatant was discarded, and the pellet resuspended in 0.8M Tris-Cl buffer solution and once again homogenized. After the homogenates were filled up to 72mL with the same solution they were transferred to the six UC-tubes, which were weighed, balanced, and centrifuged at 12.000xg, 4°C for 10 minutes. To achieve a purer myelin fraction, the supernatant was discarded and the steps from the density gradient centrifugation and osmotic shock were repeated as described above.

Lastly, two wash steps with PBS were performed. The myelin pellet after the last osmotic shock step was resuspended in 1mL of cold PBS and filled up to 12mL total volume and centrifuged at 12.000xg, 4°C for 10 minutes. Afterwards, the supernatant was discarded and 1mL of PBS was added to the first tube. The pellet was resuspended and then transferred to the next tube and so on. The result is around 1-2mL of pure myelin in PBS which was stored at –20°C.

7.4. Biochemical Analysis of myelin

7.4.1. Protein determination

The amount of protein in the myelin suspension was determined using the Pierce BCA Protein Assay Kit (Thermo Fisher Scientific). Standard curves for calibration with albumin and PBS were made to measure the protein levels as per manufacturer´s instructions. 10µL of sample (diluted or undiluted) were combined with 200µL of working solution which was prepared as per manufacturer´s instructions. After incubation of 30min at 37° in the incubator, samples were measured.

7.4.2. Western Blot

For the analysis of the myelin, two 1.5mm 10% SDS-page gels (30% acrylamide (AA), 1.5M Tris-Cl pH 8.8, 10% SDS, TEMED, 10% APS) were used. Firstly, gels were pured into BioRad chambers, then isopropanol was poured on top and the gels set for 15 minutes until hard. Then, the isopropanol was washed off with water, the collection gel (30% acrylamide (AA), 1.5M Tris-Cl pH 8.8, 10% SDS, TEMED, 10% APS) was poured on top and the combs were inserted.

7.5. Microglia isolation

The Adult Mouse Brain Dissociation Kit (130-107-677, Miltenyi Biotec) was used for the isolation of microglia from adult mice. After the brains were dissected and

weighed, they were cut into 8 sagittal sections and transferred into the MACS C tube containing an enzyme mix (as described in the kit). The tube was loaded onto the gentleMACS Dissociatior with Heaters (Miltenyi Biotec), which then performed the brain dissociation step during the on-instrument enzyme incubation. After completion of the 30-minumte dissociation, the tissue was put through a 70µm MACS SmartStrainer which was pre-moistened with D-PBS and centrifuged at 300g for 10 minutes at 4°C.

The supernatant was removed, the pellet was resuspended in 1 mL cold D-PBS and filled up to 3.1mL. 900µL of cold Debris Removal Solution was added. Further 4mL of D-PBS were added gently at a 45° angle so that the two phases do not mix. The sample was centrifuged at 1000g for 10 minutes at 4°C with no break and the upper two of three phases were removed. The tube was filled up to 10mL, inverted 3 times and centrifuged at the same parameters as before. The supernatant was removed, the pellet was resuspended in 1mL of Red Blood Cell Removal Solution and incubated for 10 minutes in the fridge. 10 mL of a D-PBS/FCS buffer (1:20) was added to the sample and centrifuged at 300g for 10 minutes at 4°C. For clarity reasons, if a buffer is mentioned in the following steps the D-PBS/FCS buffer is meant.

Myelin or O4 removal beads were used to minimize the myelin contamination in this protocol. To achieve this, the amount of myelin removal beads needed was determined by the weight of the mouse brain. The myelin beads were added to the pellet with a predetermined amount of buffer and incubated for 15 minutes in the fridge. The cells were washed by adding 10x the volume of labelling buffer and then centrifuged at 300g for 10 minutes at 4°C. The supernatant was removed completely and 1mL of buffer was added per MACS LS or LS column that was used. To magnetically separate the labelled myelin, the column was placed into a magnetic field and prepared by rinsing it with 3mL of buffer. The cell suspension was then applied onto the column and the flow-through containing the cells without the labelled myelin was collected. The column was washed two more times with 1mL of buffer each.

In the following step, the cells were labelled with CD11b+ beads, which select the microglia from the cell suspension. To achieve this, the cells were counted and per 10^7 cells, 10µL of beads were added and incubated for 15 minutes in the fridge. The cells were then washed with 1mL of buffer and centrifuged at 300g for 10 minutes

at 4°C. The magnetic separation was achieved with an MS column in a magnetic field. The column was washed with 500µL and the cell suspension was applied to the column. The flow-through was collected as the microglia-negative cell fraction. The column was removed from the magnetic field and 1mL of buffer was applied to the column and with a plunger, the labelled microglia in the column were instantly flushed out (this step was repeated to achieve higher cell number). The labelled cells were now either used for flow cytometry (FC) or cultured for the phagocytosis assay.

7.5.1. Cell culture and live imaging phagocytic assay

The isolated microglia were seeded at a concentration between 50.000 and 100.000 cells/96-well plate (Greiner, sterile, F-bottom, Cat.-No. 655180) in 7µL/well in order to achieve a drop in the middle of the well. This prohibits the cells from adhering only on the rim of the well, where they cannot be detected by the IncuCyte software. These drops are then incubated in a wet chamber for 45 minutes, before filling the wells up with 150µL DMEM complete + M-CSF medium and incubated at 37°/5% CO_2 overnight. On the next day, half of the medium was removed and filled up with 200µL of freshly prepared medium. The microglia are then cultivated without media change for 5 days before further experiments.

For the live imaging phagocytosis assay the media was removed and replaced with DMEM complete medium containing 10µg/mL WT myelin or 0.1µL of a red nuclear dye (1:1000 dilution). The plate was transferred to the IncuCyte Live-Cell Analysis System (Sartorius AG), which is placed within an incubator at 37° and 4% CO2 for up to 48 hours. The cells were allowed to settle within the system for 30 minutes to ensure successful focus of the microscope. Four pictures per well were taken every hour for the duration of the assay using a 10x objective lens. The acquisition time for the green channel (myelin uptake) was 400ms and an area filter was used to exclude objects below a certain size. The threshold for the green signal was set according to untreated cell signal and phagocytic substrate background signal. Cell segmentation was adjusted to 0.5 and the minimum phase area was set at 350µm^2, which ensured the inclusion of all single cells and the exclusion of as much debris as possible. All data was analyzed with the Incucyte software.

7.6. Flow Cytometry

The cells were used for flow cytometry analysis on the Guava easyCyte machine (serial number: 8472060245, InCyte version #3.4). The number of cells that were used for flow cytometry varied between 50.000-100.00 cells/ antibody staining, since there was a lot of variability in the isolation step. However, the volume corresponding to the same cell number/ antibody staining was maintained. The flow-through (microglia-negative fraction) and the microglia-positive fraction were each divided into four tubes, representative of the four antibodies that were used and one unstained control. They were centrifuged at 300g/5min/4°, then resuspended in 45µL PBS/FCS buffer and 1.25µL of each antibody was used. All antibodies are of the REAfinity (Miltenyi Biotec) type, which allows for only one isotype staining per wavelength used. Therefore, one sample of each fraction was stained with CD11b-APC, one with O4-PE and one with isotype APC and isotype PE (for a summary see Table 1). The samples were vortexed shortly and incubated in the fridge for 10 minutes, followed by a wash with 500µL buffer and a centrifugation at 300g/5min/4°. The supernatant was removed, and the pellet was resuspended in 350µL buffer until analysis. The gain control settings on the machine were set according using the unstained sample to determine approximate size and granularity of the cells. The following samples were then analyzed with the same settings, which can be seen in table 1.

Table 1: reagents and gain settings used for flow cytometry analysis of isolated primary microglia to establish and adapt the protocol.

Instrument: guava easyCyte		
Antibody	Fluorochrome	Vendor/Cat.No./Clone
Anti-mouse CD11b	APC	Miltenyi Biotech/#130-113-802/REA592
Anti-hu/mou/rat O4	PE	Miltenyi Biotech/#130-117-711/REA576
anti-human IgG1	APC	Miltenyi Biotech/#130-113-434/REA293
anti-human IgG1	PE	Miltenyi Biotech/#130-113-438/REA293

Gains			
FSC	108	YEL-B	336
SSC	1	RED-B	617
GRN-B	4	RED-R	456

7.7. Immunofluorescence

Primary microglia cells from 3 6JLBL6 4-week-old mice were used after 6 days of culture to achieve a representative immunofluorescence staining.

The cells were washed with 1x PBS and detached with TrypLE, which was incubated at RT for 10 minutes. Per well, 15µL DMEM complete medium was added, and the pipette tip was used to scrape off the adherent cells. All cells from each well were combined and re-plated on a round cover slip within a 24-well plate. For the first cover slip, an 80µL drop was positioned in the center of the cover slip and on the second a 60µL drop was used. The cells were then incubated to 45 minutes in the incubator and filled up with 500µL of medium and left over night. On the next day, the cover slips with adherent cells were washed with PBS and fixed with 3% paraformaldehyde (37% formaldehyde, 10x PBS and ddH_2O) for 20 minutes. Afterwards, they were washed 3 times with PBS with continuous shaking. The cells were then permeabilized and blocked with a 0.1% Triton Blocking Solution (2% FCS, 2% BSA, 0.2% fish gelatin) for 30 minutes. It should be noted, that all following antibody stainings were performed in the dark and at RT. IBA1 antibody (1:1000) was used as the first antibody and cells were incubated for 1 hour on a 100µL antibody solution (diluted with Blocking Solution) on parafilm. The cover slips were transferred to the 24-well plate again and washed 5x with PBS. The secondary antibody incubation (Cy3 donkey-anti-rabbit 1:400) was performed exactly like the first one. Another washing step with PBS was performed and lastly nuclear DAPI staining (1:1000) for 10 minutes was done. Afterwards, the cells were washed again and mowiol was used to fix the cover slip on an object slide. The slides were stored at 4° in the dark until analysis.

8. Results

8.1. Validation of microglia isolation protocol via flow cytometry

The isolation protocol for the primary microglia was adapted to our specific requirements. Cell yields of microglia ranged from 400.000 to almost 800.000 cells, and the microglia-positive fraction as well as the flow through were analyzed for percentage of microglia and myelin (O4) contamination. We first established if there is a need for the myelin-removal beads or not. Two wild type animals at the age of 3 or 4 weeks (as can be seen in table 2) were used. For WT1 myelin removal beads were used during the isolation, whereas for WT2 they were not. For WT1, the O4 contamination was 4.8% in the microglia-positive fraction and 6.9% in the flow through, whereas WT2 showed 29.5% contamination in the microglia fraction and 39.2% in the flow through. The contamination with O4+ cells in the microglia-positive fraction as well as in the flow through was noticeably higher if no myelin removal beads were used, which is visualized in figure 4.

Table 2: combined results for flow cytometry analysis of variations of the microglia isolation protocol. Usage of myelin beads improves contamination of microglia-positive fraction and age of the animal does not have noticeable effects on purity and contamination. Percentages of microglia-positive and flow through fractions stem from fully stained sample.

				Microglia-positive fraction		Flow through	
Genotype	Age (weeks)	Myelin beads	Microglia yield	CD11b+ cells (%)	O4 + cells (%)	CD11b+ cells (%)	O4 + cells (%)
WT1	3	Y	400.000	38.7	4.8	9.4	6.9
WT2	4	N	500.000	52.7	29.5	6.2	39.2
WT3	14	Y	590.000	32.5	4.5	14.5	1.2
WT4	12	Y	780.000	29.1	1.7	15.7	7.1
WT5	20	Y	480.000	92.6	2.7	0.6	0.8

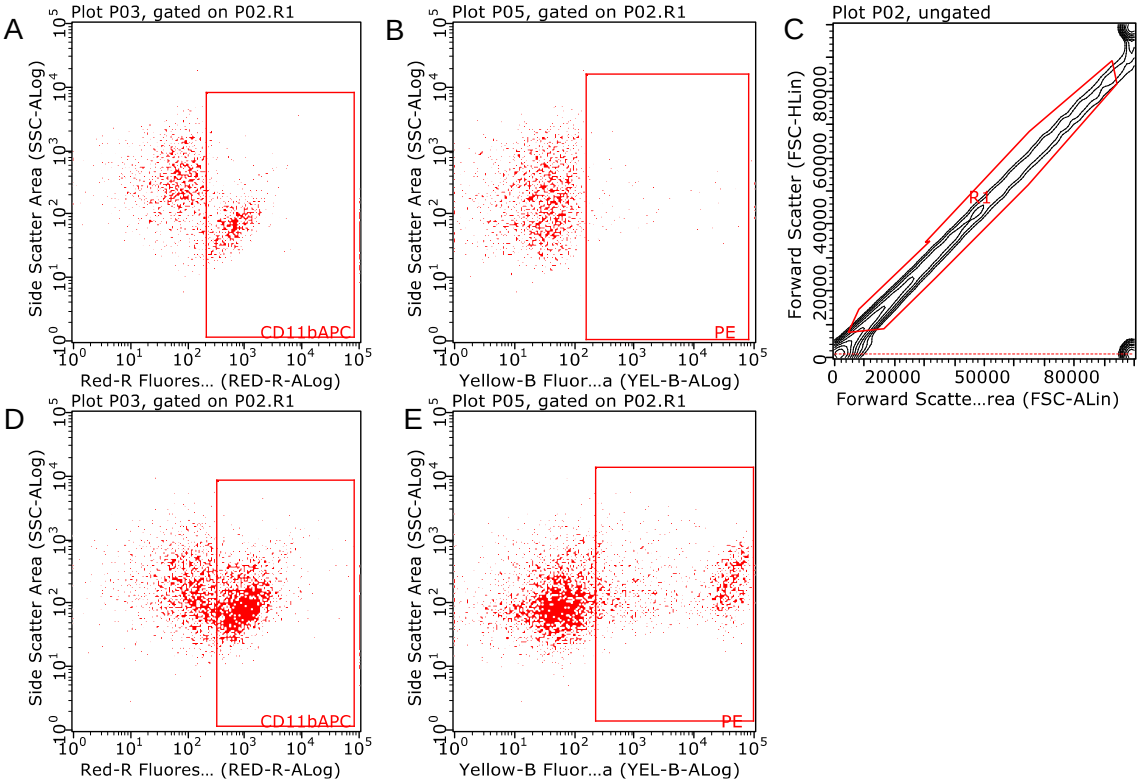

Figure 4: Preliminary testing of microglia-positive fraction regarding necessity of myelin removal through beads. A) WT1 cells show distinct CD11b+ microglia staining in the APC channel. B) O4 staining of WT1 cells show minimal contamination with myelin. C) outside of gating settings a cell population appears to distort analysis. D&E) WT2 O4 staining shows significant amount of myelin contamination in the yellow (PE) channel. It was concluded that myelin removal through beads is necessary.

After establishing the need for using O4-beads before separating the microglia, it was investigated, whether the age of the animal has an impact on the microglia cell yield and purity. As is apparent in table 2, cell yields of older animals (WT3-4) are slightly higher, however, the purity is not affected in WT3 and WT4. Since younger

animals yielded less cells and the purity is not affected significantly, all further experiments were conducted with adult mice.

Final protocol adjustments

After poor microglia purity and a relatively high percentage of microglia in the flow through for WT1-4, multiple adjustments to the protocol were made. Most significantly, the density gradient centrifugation step was identified as the most crucial step in the protocol and was therefore optimized for increased purity. Furthermore, the settings of the flow cytometer had to be adjusted. As can be seen in figure 4C, in the top left corner a cell population appeared, which showed a very high forward scatter and could not be detected by the used settings. The usage of pre-separation filters (70um) in the magnetic separation step might have dissolved cell clumps, that later appear as very large cells in the flow cytometry analysis. Following the final adaptations to the protocol, isolated microglia from two brains of 20-week-old WT mice were used to adjust the settings and further analyze the flow through and microglia-positive fraction for possible astrocyte contamination (results from this analysis can be seen in table 3). The gating strategy and consequent cell populations is shown in figure 5. An area was identified, which shows a very distinct cell population of CD11b+ cells in the microglia-positive fraction (5B), however, in the flow through no such cell population could be identified (5C). Therefore, this area (R4) was used as the gate for all further analysis. Dot plots of isotype controls were used to determine appropriate CD11b+ and O4+ gates. The observed cells shifted from isotype control samples to the stained samples successfully and the resulting dot plots and histograms can be seen in figure 5.

	Sample ID	CD11b+ fraction (%)	O4/ASC2+ fraction (%)
positive cell fraction	stained CD11b and O4	92.56	2.71
	stained ASC-2	0.84	5.12
	isotype control	1.16	1.51
	unstained	0.81	1.71
flow through	stained CD11b and O4	0.63	0.76
	stained ASC-2	0.13	51.86
	isotype control	0.29	0.19
	unstained	0.00	0.00

Table 3: percentages of cells within the gated area using InCyte software. Flow through and the positive cell fraction were analyzed according to their content of microglia-positive cells and oligodendrocyte-

This analysis shows a very high purity of microglia in the microglia-positive cell fraction and very little contamination of myelin and astrocytes. Furthermore, analysis of the flow through showed almost no CD11b+ cells, however, over 50% of astrocytes. Taken together, these findings confirm the reproducibility and success of the adapted microglia isolation protocol.

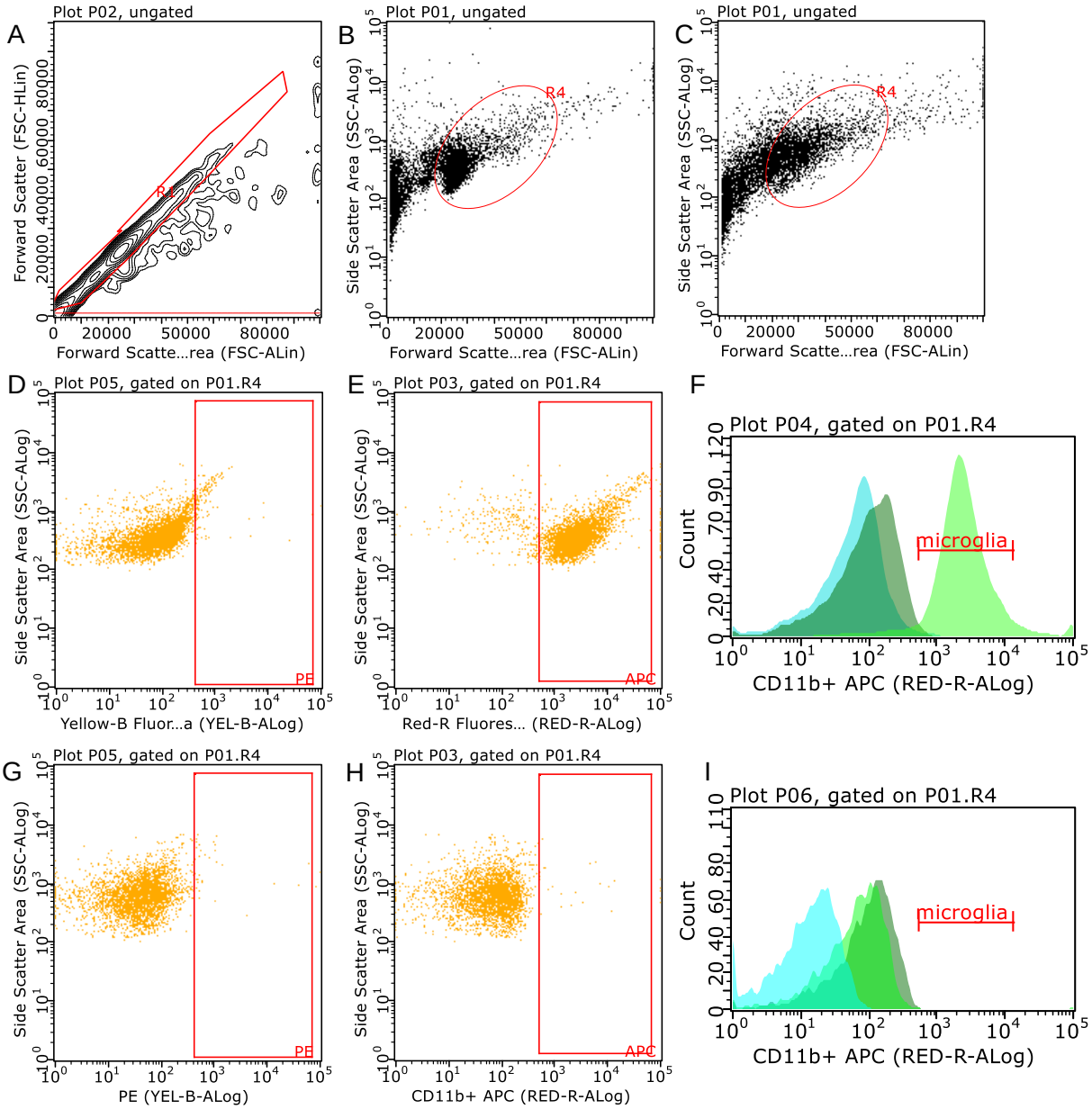

Figure 5: Flow cytometry data analysis from representative sample after successful adaptation of the microglia isolation protocol. A) contour plot of cell population indicating that correct settings were used. B) Dot plot of stained microglia fraction with R4 surrounding a very distinct cell population of microglia. C) Dot plot of stained flow through fraction where distinct cell population of B is not visible. All further analysis and plots were gated to R4. D&E) Dot plot of O4- and CD11b-positive cells of microglia fraction. F) Histogram of unstained (blue), isotype control (dark green) and microglia positive sample (bright green) in microglia positive fraction. G&H) Dot plot of O4- and CD11b-positive cells of flow through. F) Histogram of unstained (blue), isotype control (dark green) and microglia positive sample (bright green) in the flow through.

8.2. Cell culture and phagocytosis assay

8.2.1. Microglia cells are fully developed after 4 days of culture

To determine the ideal timepoint for conducting further experiments with the primary isolated microglia, they were cultured for 4 days and imaged via live-cell imaging. As is evident in figure 6, directly after isolation and after one day, the cells exhibit an amoeboid shape which is to be expected of microglia that were just isolated. On day 2 of culture, the beginning of the formation of characteristic processes can be seen and intensifies on day 3 and day 4. Despite high cell density, microglia were shown to recover from the isolation procedure and return to characteristic, healthy cell morphology on day 4 of culture. Therefore, all further experiments were conducted on day 5 of culture.

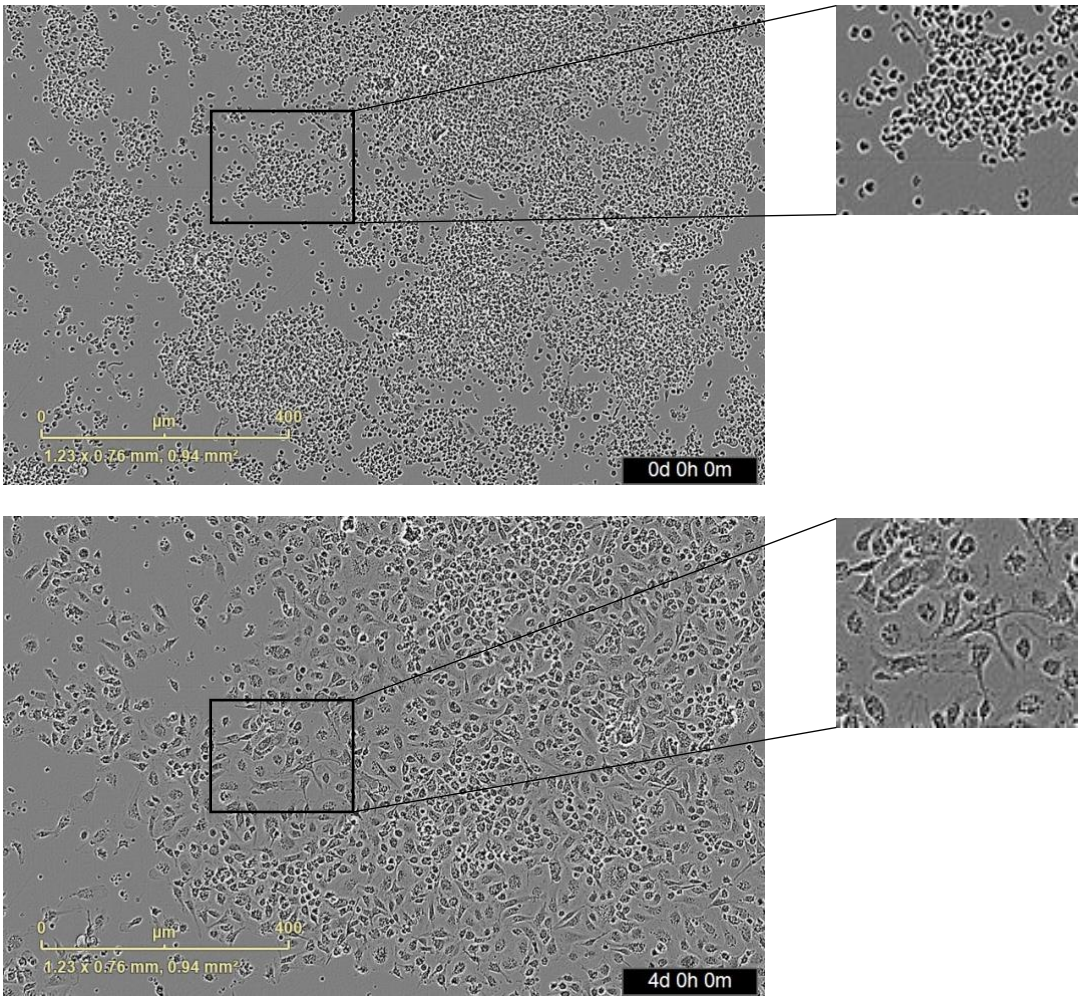

Figure 6: Increased growth and characteristic bifurcation of microglia cells in culture. Time course of isolated primary microglia cells with pHrhodo labelled myelin as a substrate of 4 days acquired with the IncuCyte software with a 10x objective (n = 1). Only day 1 and day 4 are depicted for clarity.

8.2.2. Microglia are healthy and survive during phagocytosis assay

After spending four days in culture, microglia cells were used for a phagocytosis assay in parallel with a nuclear dye staining to show the continuous survival of the cells and possibly exclude debris giving a fluorescent signal from real cells. Therefore, in three wells with a density of approximately 200.000 cells the pHrhodo labelled myelin was added as a substrate in parallel with a nuclear dye. Shown in figure 6, even when seeding the cells carefully in a 7µL drop, density of cells can vary between wells and even within one well. Furthermore, it can be said, that the nuclear dye was not taken up well by microglia in either dense or sparce seeding conditions. Despite that, the visual assessment of the cells is telling of their health and survival through the phagocytosis assay with myelin as a substrate. The nuclear dye concentration therefore is not necessary.

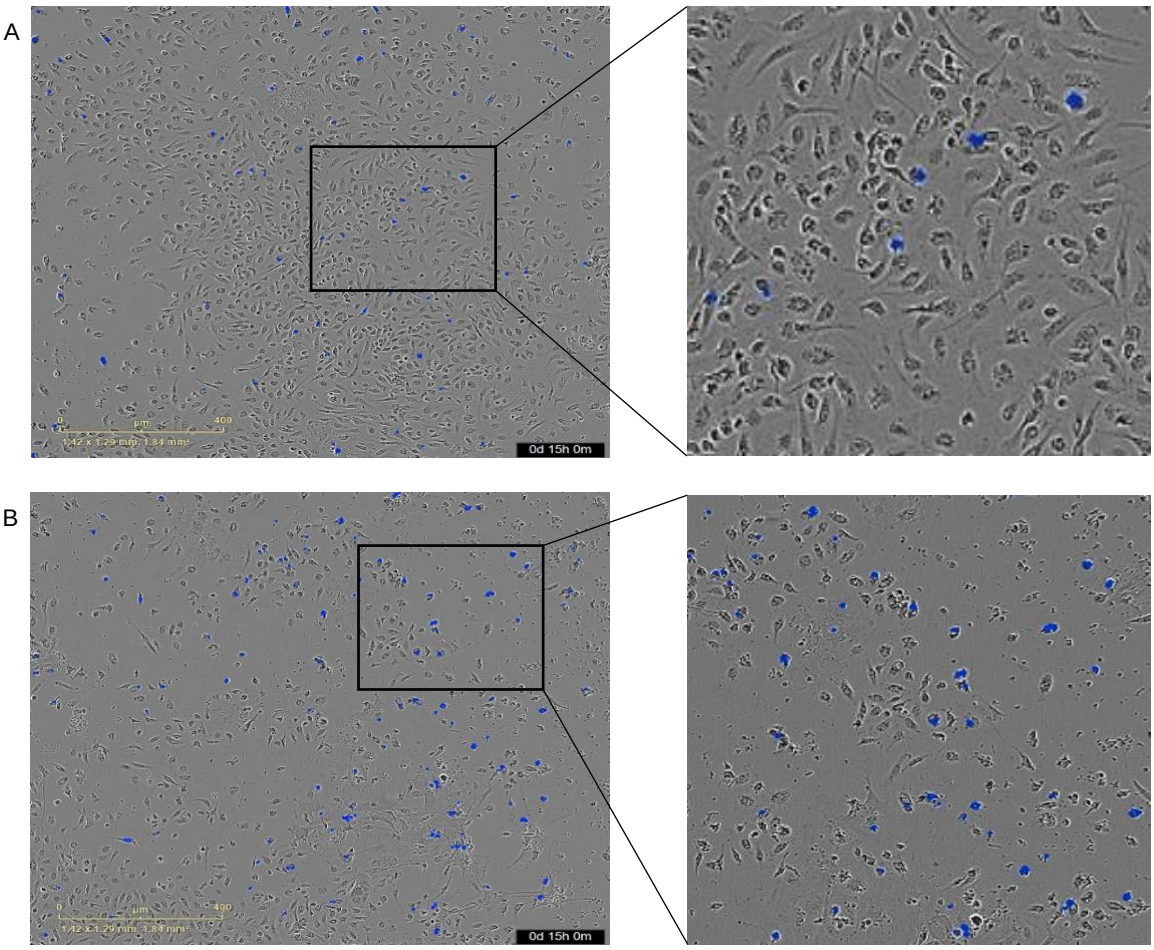

Figure 7: Nuclear dye experiment data. Blue dots represent a nuclear dye signal. A) dense cell population at 15h and 24h after adding the nuclear dye showed sparce uptake of the dye by the cells. C) less dense cell population at 15h and 24h after adding the nuclear dye show similar dye uptake patterns as dense cell populations. Dye concentration must be increased.

8.2.3. Isolated microglia are positive for IBA1 after 4 days of culture and phagocytosis assay

To investigate the prolonged survival of the isolated cells and for making certain that the isolated cells truly are microglia, immunofluorescence was conducted. These cells (n = 2) had been cultured for 4 days and subsequently went through the phagocytosis assay, which included adding myelin and red nuclear dye to the cells. After the assay, they were detached and stained for IBA1 and DAPI. As a control, half of the cells were only stained with DAPI. As can be seen in figure 8, microglia show IBA1 signal throughout their cell body. The red signal elucidates the various morphologies the microglia exhibit. At a resolution of 60x, a single cell can be observed with characteristic branched morphology and even the end point of the cell, where it attaches to the glass slide. The same can be said for a resolution of 40x, where the complete morphology of a single microglia cell is seen. At a resolution of 20x, multiple cells with varying morphologies are depicted. Smaller, rounder (also known as amoeboid) shaped cells were positive for IBA1 staining, as well as a cell with only short processes. For the control, where no IBA1 antibody was used, a red signal was detected surrounding the nucleus of the cells. Since these cells were subjected to a red nuclear dye for 48h before fixation and immunofluorescent staining, it stands to reason that these are the remnants of this nuclear dye and not an IBA1 staining. The pattern of red signal can also be clearly distinguished from the figures above, where the whole cell body is uniformly stained. However, in the control cells, the red signal only occurs directly next to the nucleus in a circular shape.

Taken together, these images confirm sustained microglia cell identity even after multiple days of culture and a 48h phagocytosis assay. This further substantiates the functionality of the suggested protocol and increases the potential applications of the protocol in various fields of interest.

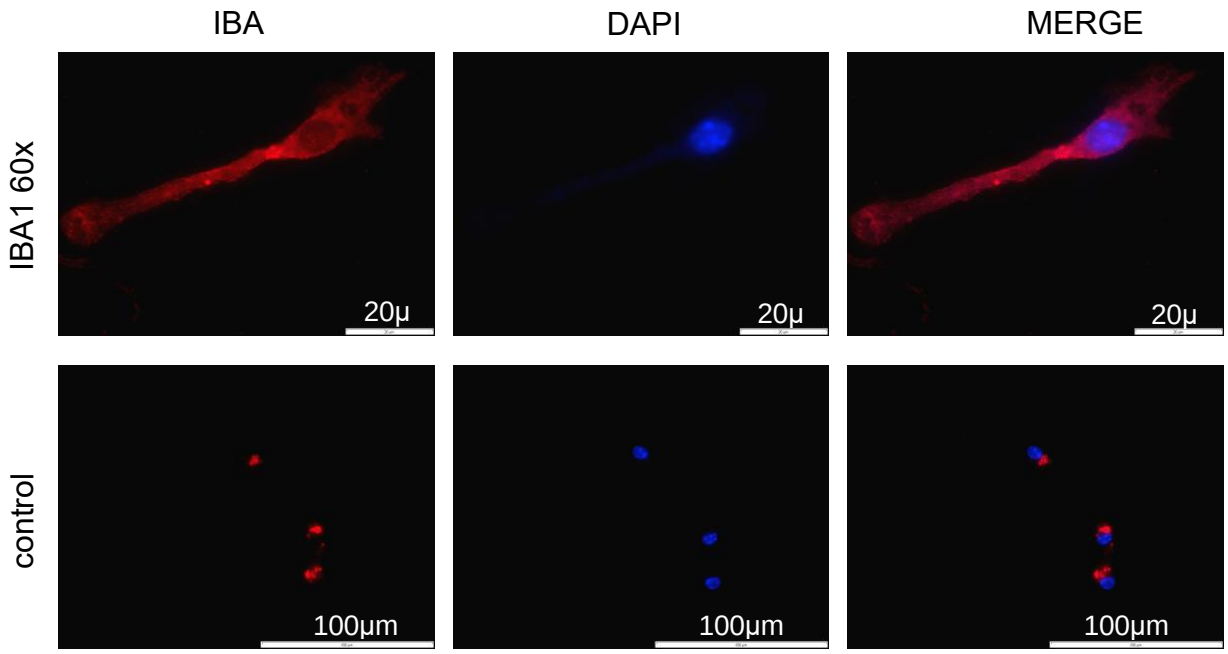

Figure 8: IBA1 and DAPI staining of primary microglia after 4 days of culture and 2 days of phagocytosis assay. Successful staining of whole microglia cell body by IBA1 confirms microglia isolation and culture protocol. The control group, where no IBA1 antibody was added shows red fluorescence, however the pattern of red staining is significantly different from IBA1 stained cells.

8.3. Primary microglia successfully phagocytose WT myelin

As phagocytosis of myelin is one of the key functions of microglia in the CNS, it was pivotal to show proper phagocytosis function of the isolated microglia. To achieve this, microglia were left for 4 days in culture and phagocytosis activity was measured for 48 in case of late-onset phagocytosis. The live cell-imaging software measured the green area relative to the phase area, giving relevant fluorescent signal intensity of the primary microglia. As can be seen in figure 9, the primary microglia showed successful phagocytosis ability of WT myelin labelled with pHrhodo green dye. Green dots and lines in the figure represent either the relative fluorescent signal of the replicates combined (9A) or separately (9B). In red cells without myelin addition are depicted and in blue the background signal is shown, which consists of only myelin but no cells. The bars of each dot show the standard deviation of each well. Phagocytosis of myelin showed a similar pattern in all three replicates; however, the intensity of green, fluorescent signal is overall rather low. Highest fluorescent signal occurred between 12 and 15 hours after myelin addition and continues to drop off in a linear way after these timepoints. A renewed increase in signal was registered at 45 hours, however, due to the overall pattern of phagocytosis and comparisons

to the current literature, this seems to be an artefact of some sort rather than a true increase in phagocytosis activity. Regarding the untreated control, a complete drop in in fluorescent signal was observed at timepoints 20, 24, 30 and 41 hours. At these timepoints, the IncuCyte took out-of-focus images of the well, explaining the unusual pattern in this case.

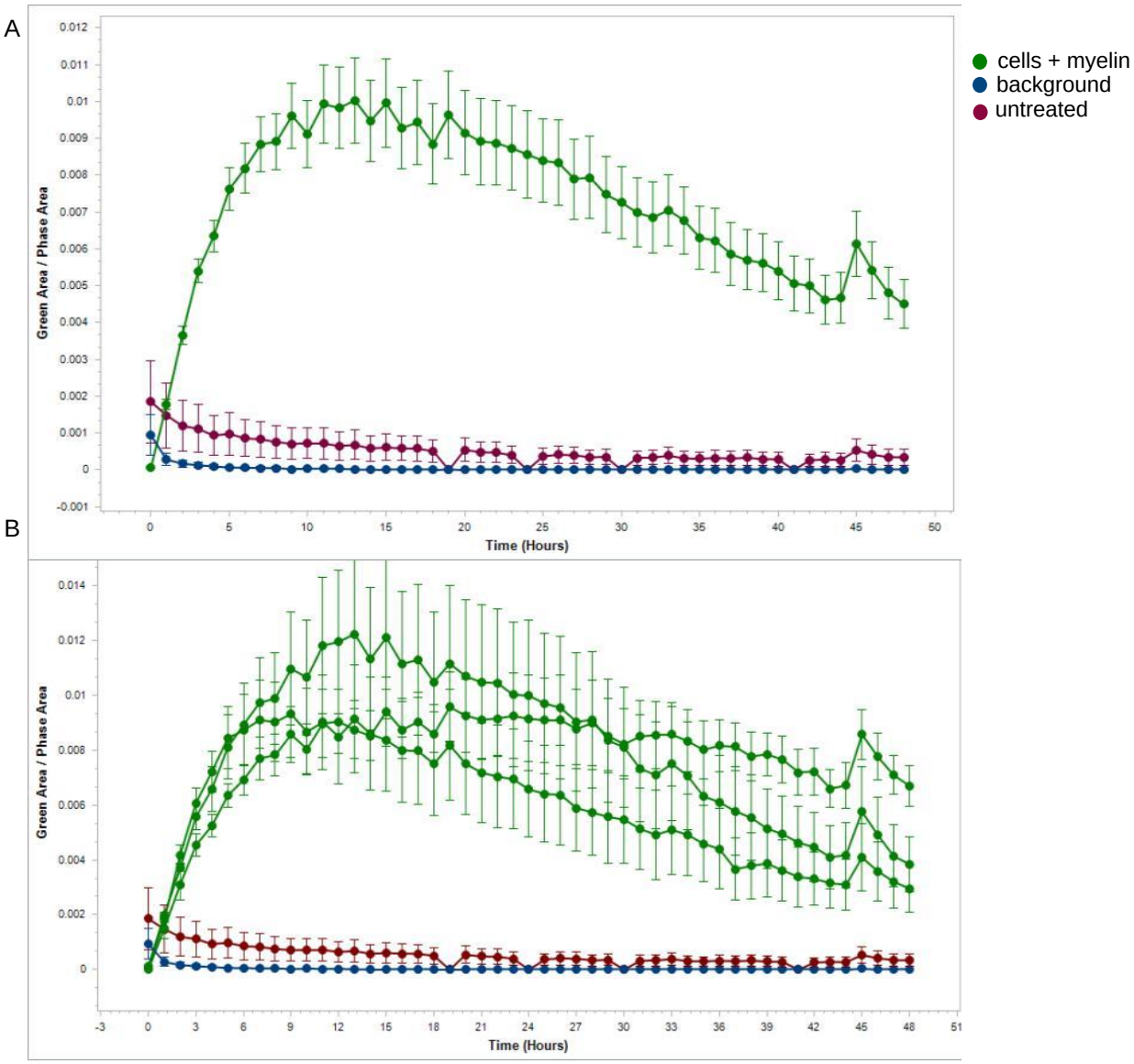

Figure 9: Results of myelin phagocytosis by primary microglia over 48h. Cells of two brains were combined and seeded in three wells including a background control for the fluorescent myelin and ar untreated control. A) results of the ratio of green area vs. phase area for 3 wells filled with cells and myelin replicates combined including standard error bars. B) green area/phase area for each of the replicates

These results indicate successful phagocytosis ability of the isolated primary microglia and an overall relatively low fluorescent signal, with the highest phagocytosis rate between 12 and 15 hours after myelin addition.

9. Discussion

The absence of ether lipids in humans has been associated with the manifestation of RCDP, a debilitating and infrequent genetic disorder characterized by severe skeletal abnormalities and impaired growth. Only 50% of patients born with this disease make it to 6 years of age, before the disease kills them (Braverman & Moser, 2012b). Microglia, the resident immune cells of the central nervous system, are recognized for their pivotal role in the clearance of cellular debris following demyelination and synaptic pruning during neural development. This thesis was undertaken with the objective of establishing a robust methodology for the isolation of primary microglia derived from adult murine brains. The outcome of this thesis is the a reliable protocol for the extraction and purification of these cells, the outcomes are anticipated to facilitate subsequent investigations involving microglia. Such advancements hold promise for interdisciplinary applications, spanning fields ranging from neurobiology to immunology, thereby augmenting the scientific understanding of microglial function and its implications in various pathological contexts. Here, we discuss the implications of our findings and the significance of the established method in the context of ether lipid deficiencies.

9.1. Validation and Adaptation of Microglia Isolation Protocol

As a first step in our initial validation experiments, we determined the importance of incorporating myelin removal beads into the isolation protocol. Manufacturing instructions (Miltenyi) indicated a necessity for myelin removal beads, however, several publications with similar aims emphasized the density gradient centrifugation step as most important (Bohlen et al., 2019; Bordt et al., 2020). The significant reduction in myelin contamination observed when using myelin removal beads in this study underscores their necessity in achieving high-purity microglia populations. Since the usage of myelin removal beads did not significantly change the achieved cell numbers, we proceeded the experiments with myelin removal beads. It should be noted, however, that the duration of the isolation protocol is increased by approximately 30 minutes, possibly impacting the quality of the isolated microglia.

Furthermore, our analysis of the effect of animal age on microglia isolation yielded valuable insights. While most publications into the topic of primary microglia isolation repeatedly emphasized the importance of neonatal or very young animals,

citing myelin contamination and microglia quality as their main motive. In these cases, the protocol for isolating microglia entails significantly longer durations, shaking-off of the microglia and increased time for culture (Li et al., 2022). These protocols were not applicable in this study for several reasons. Firstly, obtaining neonatal mouse brains requires not only impeccable timing but also specialized skills. Secondly, the mortality rate of newborn *Gnpat* KO mice is high, with breeding in general proving difficult. Thirdly, the pathologies of the mice are intensified in progressed age with some of the pathologies only developing after adolescence. The overall aim of the study being to investigate possible microglia dysfunctions in these pathologies, it was important to extract the microglia at a time where the full progression of disease had been reached. Therefore, using adult animals was the more practical as well as sensible approach. In our analysis we found that older animals demonstrated slightly higher cell yields, however, the purity of microglia cells remained consistent across 3-4-week-old and up to 20 weeks old animals. This finding supports the use of adult mice for further experiments, ensuring sufficient cell yields without compromising purity. Our purity of approximately 93% ties in with publications where purity ranges between 90%-95%, depending on the method of isolation (Bordt et al., 2020; Liu et al., 2006). However, it's worth noting that variations in microglia yield and purity may arise from factors beyond animal age, such as genetic background or experimental conditions.

Striving to optimization of the protocol led to several crucial adjustments aimed at enhancing isolation efficiency and purity. The optimization of density gradient centrifugation and fine-tuning of flow cytometer settings proved instrumental in improving the overall purity of microglia isolates. Our average purity of These adjustments not only addressed the observed contamination issues but also contributed to the reproducibility and reliability of the isolation protocol. Moreover, the gating strategy of distinct cell populations using flow cytometry enabled accurate quantification of microglia purity and contamination levels.

9.2. Functional Assessment of Isolated Microglia

The subsequent functional assessment of isolated microglia through cell culture, immunofluorescence and phagocytosis assays provided additional validation of the established protocol. After we achieved successful flow cytometry results, the next obstacle was determining optimal culture conditions and durations. Once again,

some publications with similar aims used very different culture conditions. Most used a specific Microglia Growth Medium (either commercially bought or tediously made), which requires a multitude of ingredients which are not usually found in a lab, therefore making it expensive or time intensive to produce (Bohlen et al., 2017). Before investing such amounts of funds or time, we aimed at achieving similar culture conditions with standard equipment and cell culture solutions already available in the lab. The nature of our isolation protocol made it so that the microglia did not have to further differentiate or multiply in our culture conditions, they only needed to recover from the isolation process and take their characteristic form. It is for that reason why our growth medium consisted only of DMEM complete and MCSF, which was sufficient to achieve our goal.

The time-course analysis of phagocytosis revealed distinct peak activity patterns for WT microglia. Specifically, our results demonstrated that in our primary microglia cells, the peak of phagocytosis occurred approximately 12-15 hours after the addition of labelled myelin particles. In contrast, a study using a microglia BV-2 cell line exhibited a delayed peak, with maximal phagocytic activity observed at 22-24 hours post-stimulation with myelin particles (Zorina et al., 2018). Interestingly, in microglia infected with prions, a significant upregulation of phagocytosis could be observed, reaching its peak as early as 6 hours after myelin addition (Sinha et al., 2021). These findings underscore the dynamic nature of microglial phagocytosis and highlight the impact of different experimental conditions on its temporal dynamics. Furthermore, our results also revealed a lower level of phagocytosis in primary microglia compared to those of a BV2 cell line (Zorina et al., 2018). One potential explanation for this discrepancy could be the density at which the cells were seeded. It is plausible that primary microglia cells were seeded at a higher density, which may have influenced their phagocytic activity. Further investigation into the seeding density and its effect on phagocytosis is warranted to elucidate this observation fully. It is also known, that cell lines of any kind perform better in functional assays than primary cells. The ability of our isolated microglia to take up myelin particles, albeit at low levels, is indicative of successful isolation and culture conditions.

9.3. Limitations

This study's sample size was relatively small, consisting of wild-type animals of varying ages, which may limit the generalizability of the findings. Future research could enhance the robustness of the method by including a larger and more diverse sample population. While the study primarily focused on establishing and validating a microglia isolation protocol via flow cytometry, its efficacy and limitations may vary across different experimental setups and research questions. Thus, further investigation is warranted to assess its suitability for alternative experimental designs or downstream analyses. While efforts were made to optimize the isolation protocol and minimize contamination, reliance solely on flow cytometry analysis may not provide a comprehensive assessment of all potential impurities. Incorporating complementary techniques such as RNA analysis or gene expression analysis could provide additional insights into purity and contamination sources. The phagocytosis assay's reliance on pHrhodo-labelled myelin particles presents limitations in sensitivity and specificity, with variations in assay conditions potentially affecting outcomes. Further characterization of phagocytosis kinetics and specificity could enhance the assay's reliability and relevance to physiological microglial function.

9.4. Implications and Future Directions

The successful establishment and validation of a robust microglia isolation protocol from adult mouse brains have far-reaching implications for neuroimmunology research. The high-purity microglia populations obtained from adult brains using this protocol offer a reliable platform for investigating various aspects of microglia biology, including their roles in neuroinflammation, synaptic remodeling, and neurodegenerative diseases.

Future research endeavors may explore the applicability of the established protocol in studying microglia heterogeneity across different brain regions or disease models. Additionally, further optimization and validation of the protocol for specific experimental contexts, such as single-cell RNA sequencing or spatial transcriptomics, could enhance our understanding of microglia function at the molecular level.

In conclusion, the findings presented in this study underscore the importance of methodological standardization in microglia isolation and provide a foundation for advancing our knowledge of microglia biology in health and disease. By establishing a reliable and reproducible isolation protocol, this study contributes to the methodological toolkit available to researchers in the field of neuroimmunology, paving the way for future discoveries and therapeutic interventions targeting microglia-mediated pathologies.

10. References

Aggarwal, S., Yurlova, L., & Simons, M. (2011). Central nervous system myelin: Structure, synthesis and assembly. *Trends in Cell Biology*, *21*(10), 585–593. https://doi.org/10.1016/j.tcb.2011.06.004

Ali, F., Hossain, Md. S., Abdeen, A., Uddin, Md. S., Gaber, A., Alsanie, W. F., Waheed, R., Shanab, O., & Ahmed, H. (2022). Plasmalogens ensure the stability of non-neuronal (microglial) cells during long-term cytotoxicity. *Environmental Science and Pollution Research*, *29*(2), 2084–2097. https://doi.org/10.1007/s11356-021-15773-7

Ali, F., Hossain, Md. S., Sejimo, S., & Akashi, K. (2019). Plasmalogens Inhibit Endocytosis of Toll-like Receptor 4 to Attenuate the Inflammatory Signal in Microglial Cells. *Molecular Neurobiology*, *56*(5), 3404–3419. https://doi.org/10.1007/s12035-018-1307-2

Alkan, A., Kutlu, R., Yakinci, C., Sigirci, A., Aslan, M., & Sarac, K. (2003). Delayed myelination in a rhizomelic chondrodysplasia punctata case: MR spectroscopy findings. *Magnetic Resonance Imaging*, *21*(1), 77–80. https://doi.org/10.1016/S0730-725X(02)00625-2

Barøy, T., Koster, J., Strømme, P., Ebberink, M. S., Misceo, D., Ferdinandusse, S., Holmgren, A., Hughes, T., Merckoll, E., Westvik, J., Woldseth, B., Walter, J., Wood, N., Tvedt, B., Stadskleiv, K., Wanders, R. J. A., Waterham, H. R., & Frengen, E. (2015). A novel type of rhizomelic chondrodysplasia punctata, RCDP5, is caused by loss of the PEX5 long isoform. *Human Molecular Genetics*, *24*(20), 5845–5854. https://doi.org/10.1093/hmg/ddv305

Bellesi, M., De Vivo, L., Chini, M., Gilli, F., Tononi, G., & Cirelli, C. (2017). Sleep Loss Promotes Astrocytic Phagocytosis and Microglial Activation in Mouse Cerebral Cortex. *The Journal of Neuroscience*, *37*(21), 5263–5273. https://doi.org/10.1523/JNEUROSCI.3981-16.2017

Björn M van Geel, Johanna Assies, Ronald J A Wanders, & Peter G Barth. (1997). X linked adrenoleukodystrophy: Clinical presentation, diagnosis, and therapy. *Journal of Neurology, Neurosurgery & Psychiatry*, *63*(1), 4. https://doi.org/10.1136/jnnp.63.1.4

Bogie, J. F., Stinissen, P., Hellings, N., & Hendriks, J. J. (2011). Myelin-phagocytosing macrophages modulate autoreactive T cell proliferation. *Journal of Neuroinflammation*, *8*(1), 85. https://doi.org/10.1186/1742-2094-8-85

Bohlen, C. J., Bennett, F. C., & Bennett, M. L. (2019). Isolation and Culture of Microglia. *Current Protocols in Immunology*, *125*(1), e70. https://doi.org/10.1002/cpim.70

Bohlen, C. J., Bennett, F. C., Tucker, A. F., Collins, H. Y., Mulinyawe, S. B., & Barres, B. A. (2017). Diverse Requirements for Microglial Survival, Specification, and Function Revealed by Defined-Medium Cultures. *Neuron*, *94*(4), 759-773.e8. https://doi.org/10.1016/j.neuron.2017.04.043

Bordt, E. A., Block, C. L., Petrozziello, T., Sadri-Vakili, G., Smith, C. J., Edlow, A. G., & Bilbo, S. D. (2020). Isolation of Microglia from Mouse or Human Tissue. *STAR Protocols*, *1*(1), 100035. https://doi.org/10.1016/j.xpro.2020.100035

Braverman, N. E., & Moser, A. B. (2012a). Functions of plasmalogen lipids in health and disease. *Biochimica et Biophysica Acta (BBA) - Molecular Basis*

of Disease, *1822*(9), 1442–1452. https://doi.org/10.1016/j.bbadis.2012.05.008

Braverman, N. E., & Moser, A. B. (2012b). Functions of plasmalogen lipids in health and disease. *Biochimica et Biophysica Acta (BBA) - Molecular Basis of Disease*, *1822*(9), 1442–1452. https://doi.org/10.1016/j.bbadis.2012.05.008

Chung, W.-S., Clarke, L. E., Wang, G. X., Stafford, B. K., Sher, A., Chakraborty, C., Joung, J., Foo, L. C., Thompson, A., Chen, C., Smith, S. J., & Barres, B. A. (2013). Astrocytes mediate synapse elimination through MEGF10 and MERTK pathways. *Nature*, *504*(7480), 394–400. https://doi.org/10.1038/nature12776

Chung, W.-S., Verghese, P. B., Chakraborty, C., Joung, J., Hyman, B. T., Ulrich, J. D., Holtzman, D. M., & Barres, B. A. (2016). Novel allele-dependent role for APOE in controlling the rate of synapse pruning by astrocytes. *Proceedings of the National Academy of Sciences*, *113*(36), 10186–10191. https://doi.org/10.1073/pnas.1609896113

Dorninger, F., Brodde, A., Braverman, N. E., Moser, A. B., Just, W. W., Forss-Petter, S., Brügger, B., & Berger, J. (2015). Homeostasis of phospholipids—The level of phosphatidylethanolamine tightly adapts to changes in ethanolamine plasmalogens. *Biochimica et Biophysica Acta (BBA) - Molecular and Cell Biology of Lipids*, *1851*(2), 117–128. https://doi.org/10.1016/j.bbalip.2014.11.005

Dorninger, F., Forss-Petter, S., Wimmer, I., & Berger, J. (2020). Plasmalogens, platelet-activating factor and beyond – Ether lipids in signaling and

neurodegeneration. *Neurobiology of Disease*, *145*, 105061. https://doi.org/10.1016/j.nbd.2020.105061

Dorninger, F., Gundacker, A., Zeitler, G., Pollak, D. D., & Berger, J. (2019). Ether Lipid Deficiency in Mice Produces a Complex Behavioral Phenotype Mimicking Aspects of Human Psychiatric Disorders. *International Journal of Molecular Sciences*, *20*(16), 3929. https://doi.org/10.3390/ijms20163929

Dorninger, F., König, T., Scholze, P., Berger, M. L., Zeitler, G., Wiesinger, C., Gundacker, A., Pollak, D. D., Huck, S., Just, W. W., Forss-Petter, S., Pifl, C., & Berger, J. (2019). Disturbed neurotransmitter homeostasis in ether lipid deficiency. *Human Molecular Genetics*, *28*(12), 2046–2061. https://doi.org/10.1093/hmg/ddz040

Duker, A. L., Niiler, T., Eldridge, G., Brereton, N. H., Braverman, N. E., & Bober, M. B. (2017). Growth charts for individuals with rhizomelic chondrodysplasia punctata. *American Journal of Medical Genetics Part A*, *173*(1), 108–113. https://doi.org/10.1002/ajmg.a.37961

Duker, A. L., Niiler, T., Kinderman, D., Schouten, M., Poll-The, B. T., Braverman, N., & Bober, M. B. (2020). Rhizomelic chondrodysplasia punctata morbidity and mortality, an update. *American Journal of Medical Genetics Part A*, *182*(3), 579–583. https://doi.org/10.1002/ajmg.a.61413

Filipello, F., Morini, R., Corradini, I., Zerbi, V., Canzi, A., Michalski, B., Erreni, M., Markicevic, M., Starvaggi-Cucuzza, C., Otero, K., Piccio, L., Cignarella, F., Perrucci, F., Tamborini, M., Genua, M., Rajendran, L., Menna, E., Vetrano, S., Fahnestock, M., … Matteoli, M. (2018). The Microglial Innate Immune Receptor TREM2 Is Required for Synapse Elimination and Normal Brain

Connectivity. *Immunity*, *48*(5), 979-991.e8. https://doi.org/10.1016/j.immuni.2018.04.016

Flannagan, R. S., Jaumouillé, V., & Grinstein, S. (2012). The Cell Biology of Phagocytosis. *Annual Review of Pathology: Mechanisms of Disease*, *7*(1), 61–98. https://doi.org/10.1146/annurev-pathol-011811-132445

Galloway, D. A., Phillips, A. E. M., Owen, D. R. J., & Moore, C. S. (2019). Phagocytosis in the Brain: Homeostasis and Disease. *Frontiers in Immunology*, *10*. https://www.frontiersin.org/articles/10.3389/fimmu.2019.00790

Han, X. (2005). Lipid alterations in the earliest clinically recognizable stage of Alzheimer's disease: Implication of the role of lipids in the pathogenesis of Alzheimer's disease. *Current Alzheimer Research*, *2*(1), 65–77. https://doi.org/10.2174/1567205052772786

Han, X., Holtzman, D. M., & McKeel Jr., D. W. (2001). Plasmalogen deficiency in early Alzheimer's disease subjects and in animal models: Molecular characterization using electrospray ionization mass spectrometry. *Journal of Neurochemistry*, *77*(4), 1168–1180. Scopus. https://doi.org/10.1046/j.1471-4159.2001.00332.x

Honsho, M., Asaoku, S., Fukumoto, K., & Fujiki, Y. (2013). Topogenesis and Homeostasis of Fatty Acyl-CoA Reductase 1*. *Journal of Biological Chemistry*, *288*(48), 34588–34598. https://doi.org/10.1074/jbc.M113.498345

Ingham, N. J., Pearson, S. A., Vancollie, V. E., Rook, V., Lewis, M. A., Chen, J., Buniello, A., Martelletti, E., Preite, L., Lam, C. C., Weiss, F. D., Powis, Z., Suwannarat, P., Lelliott, C. J., Dawson, S. J., White, J. K., & Steel, K. P.

(2019). Mouse screen reveals multiple new genes underlying mouse and human hearing loss. *PLOS Biology*, *17*(4), e3000194. https://doi.org/10.1371/journal.pbio.3000194

Kopper, T. J., & Gensel, J. C. (2018). Myelin as an inflammatory mediator: Myelin interactions with complement, macrophages, and microglia in spinal cord injury. *Journal of Neuroscience Research*, *96*(6), 969–977. https://doi.org/10.1002/jnr.24114

Li, S., Wernersbach, I., Harms, G. S., & Schäfer, M. K. E. (2022). Microglia subtypes show substrate- and time-dependent phagocytosis preferences and phenotype plasticity. *Frontiers in Immunology*, *13*, 945485. https://doi.org/10.3389/fimmu.2022.945485

Liu, Y., Hao, W., Letiembre, M., Walter, S., Kulanga, M., Neumann, H., & Fassbender, K. (2006). Suppression of Microglial Inflammatory Activity by Myelin Phagocytosis: Role of p47-PHOX-Mediated Generation of Reactive Oxygen Species. *Journal of Neuroscience*, *26*(50), 12904–12913. https://doi.org/10.1523/JNEUROSCI.2531-06.2006

Mapstone, M., Cheema, A. K., Fiandaca, M. S., Zhong, X., Mhyre, T. R., MacArthur, L. H., Hall, W. J., Fisher, S. G., Peterson, D. R., Haley, J. M., Nazar, M. D., Rich, S. A., Berlau, D. J., Peltz, C. B., Tan, M. T., Kawas, C. H., & Federoff, H. J. (2014). Plasma phospholipids identify antecedent memory impairment in older adults. *Nature Medicine*, *20*(4), Article 4. https://doi.org/10.1038/nm.3466

Roberts, A. W., Lee, B. L., Deguine, J., John, S., Shlomchik, M. J., & Barton, G. M. (2017). Tissue-Resident Macrophages Are Locally Programmed for Silent

Clearance of Apoptotic Cells. *Immunity*, *47*(5), 913-927.e6. https://doi.org/10.1016/j.immuni.2017.10.006

Rodemer, C., Thai, T.-P., Brugger, B., Kaercher, T., Werner, H., Nave, K.-A., Wieland, F., Gorgas, K., & Just, W. W. (2003). Inactivation of ether lipid biosynthesis causes male infertility, defects in eye development and optic nerve hypoplasia in mice. *Human Molecular Genetics*, *12*(15), 1881–1895. Scopus. https://doi.org/10.1093/hmg/ddg191

Rubio, J. M., Astudillo, A. M., Casas, J., Balboa, M. A., & Balsinde, J. (2018). Regulation of Phagocytosis in Macrophages by Membrane Ethanolamine Plasmalogens. *Frontiers in Immunology*, *9*, 1723. https://doi.org/10.3389/fimmu.2018.01723

Schafer, D. P., & Stevens, B. (2013). Phagocytic glial cells: Sculpting synaptic circuits in the developing nervous system. *Current Opinion in Neurobiology*, *23*(6), 1034–1040. https://doi.org/10.1016/j.conb.2013.09.012

Sinha, A., Kushwaha, R., Molesworth, K., Mychko, O., Makarava, N., & Baskakov, I. V. (2021). Phagocytic Activities of Reactive Microglia and Astrocytes Associated with Prion Diseases Are Dysregulated in Opposite Directions. *Cells*, *10*(7), Article 7. https://doi.org/10.3390/cells10071728

Sipe, G. O., Lowery, R. L., Tremblay, M.-È., Kelly, E. A., Lamantia, C. E., & Majewska, A. K. (2016). Microglial P2Y12 is necessary for synaptic plasticity in mouse visual cortex. *Nature Communications*, *7*(1), 10905. https://doi.org/10.1038/ncomms10905

Smith, J. J., & Aitchison, J. D. (2013). Peroxisomes take shape. *Nature Reviews Molecular Cell Biology*, *14*(12), 803–817. https://doi.org/10.1038/nrm3700

Stephan, A. H., Barres, B. A., & Stevens, B. (2012). The Complement System: An Unexpected Role in Synaptic Pruning During Development and Disease. *Annual Review of Neuroscience*, *35*(1), 369–389. https://doi.org/10.1146/annurev-neuro-061010-113810

Wanders, R. J. A., & Waterham, H. R. (2006). Biochemistry of Mammalian Peroxisomes Revisited. *Annual Review of Biochemistry*, *75*(1), 295–332. https://doi.org/10.1146/annurev.biochem.74.082803.133329

Wang, X., Cao, K., Sun, X., Chen, Y., Duan, Z., Sun, L., Guo, L., Bai, P., Sun, D., Fan, J., He, X., Young, W., & Ren, Y. (2015). Macrophages in spinal cord injury: Phenotypic and functional change from exposure to myelin debris. *Glia*, *63*(4), 635–651. https://doi.org/10.1002/glia.22774

Waterham, H. R., & Ebberink, M. S. (2012). Genetics and molecular basis of human peroxisome biogenesis disorders. *Biochimica et Biophysica Acta (BBA) - Molecular Basis of Disease*, *1822*(9), 1430–1441. https://doi.org/10.1016/j.bbadis.2012.04.006

Werner, E. R., Keller, M. A., Sailer, S., Lackner, K., Koch, J., Hermann, M., Coassin, S., Golderer, G., Werner-Felmayer, G., Zoeller, R. A., Hulo, N., Berger, J., & Watschinger, K. (2020). The TMEM189 gene encodes plasmanylethanolamine desaturase which introduces the characteristic vinyl ether double bond into plasmalogens. *Proceedings of the National Academy of Sciences*, *117*(14), 7792–7798. https://doi.org/10.1073/pnas.1917461117

Zorina, Y., Stricker, J., Caggiano, A. O., & Button, D. C. (2018). Human IgM antibody rHIgM22 promotes phagocytic clearance of myelin debris by

microglia. *Scientific Reports*, *8*(1), Article 1. https://doi.org/10.1038/s41598-018-27559-y